

Giant Anomalous Hall Conductivity at the Pt/Cr₂O₃ Interface


Takahiro Moriyama^{1,*}, Yu Shiratsuchi^{2,†}, Tatsuya Iino¹, Hikaru Aono², Motohiro Suzuki³, Tetsuya Nakamura³, Yoshinori Kotani³, Ryoichi Nakatani², Kohji Nakamura⁴, and Teruo Ono¹

¹*Institute for Chemical Research, Kyoto University, Uji, Kyoto 611-0011, Japan*

²*Graduate School of Engineering, Osaka University, Suita, Osaka 565-0871, Japan*

³*Japan Synchrotron Radiation Research Institute (JASRI), Sayo, Hyogo 679-5198, Japan*

⁴*Department of Physics Engineering, Mie University, Tsu, Mie 514-8507, Japan*

 (Received 29 August 2019; revised manuscript received 26 January 2020; accepted 3 March 2020; published 20 March 2020)

The interface between a magnetic material and a heavy metal that has a large spin-orbit interaction is at the root of various spin-related phenomena. In this paper, we address the peculiar spin-dependent transport at a Pt/Cr₂O₃ interface by exploring the origin of the nonlinear anomalous Hall effect (AHE) in Pt/Cr₂O₃ bilayers. X-ray magnetic circular dichroism (XMCD) measurements show no appreciable magnetic moment at the interface originating from Cr 3*d* and Pt 5*d* orbitals, which could be associated with the AHE response. A possible interfacial magnetic moment M at the Pt/Cr₂O₃ interface, assumed from the detection limit of the XMCD measurements, yields an anomalous Hall conductivity (σ_{AHE}) per unit net magnetic moment (M), $-\sigma_{\text{AHE}}/M$, of 0.57 V^{-1} , which is extraordinary large compared with that for general magnetic materials. Together with first-principles calculations, the results suggest the possibility of an intrinsic AHE in the Pt/Cr₂O₃ interface that does not rely on the net magnetic moment.

DOI: [10.1103/PhysRevApplied.13.034052](https://doi.org/10.1103/PhysRevApplied.13.034052)

I. INTRODUCTION

There is growing interest in spin-dependent transport due to the Berry phase and topological effects, manifested by the anomalous Hall effect (AHE) [1,2]. The magnitude of the AHE has been phenomenologically believed to be proportional to the magnitude of the spontaneous magnetization. However, since the intrinsic AHE emerges from an interplay between the Berry curvature and the spin-orbit coupling, a spontaneous magnetization is not always necessary for the AHE to occur. There are a few important examples which experimentally demonstrate such an interplay in the AHE. The itinerant ferromagnetic oxide SrRuO₃ is one of the typical materials which exhibit an intrinsic AHE, due to a strong spin-orbit interaction [3,4] together with a Berry curvature associated with multiple band crossings around the Fermi level E_F . One can observe a nonzero anomalous Hall conductivity when the net magnetization is zero. Another example is the antiferromagnetic material Mn₃Sn, with a chiral Kagome magnetic lattice [5]. While it has a negligibly small net magnetization, a sizable AHE has been observed due to the Berry curvature associated with the spin-chiral texture. A similar giant AHE has been predicted and observed in the

Mn₃X family ($X = \text{Sn, Ge, Ir, Pt, etc.}$) [6,7]. Both of these examples manifest the effects of the Berry phase and the spin-orbit interaction on the bulk properties.

On the other hand, interfaces between a magnetic material and a heavy metal (HM) that has a large spin-orbit coupling exhibit a variety of spin-related interfacial phenomena, such as proximity-induced magnetic moments [8–10], the Dzyaloshinskii-Moriya interaction [11], the Rashba effect [12], and spin-orbit torque [13,14]. These phenomena have been of great importance in spintronic applications, as interfacial engineering can drastically improve the properties of devices and add novel functionalities. However, although these phenomena are recognized to be phenomenologically useful, the detailed physical mechanisms of how they occur are still controversial, partly due to experimental difficulties rooted in the nature of the interfaces. One of the intriguing consequences of these phenomena is a novel type of interfacial magnetoresistance in HM/magnetic material bilayer systems, the so-called spin Hall magnetoresistance (SMR) [15,16], that is induced in conjunction with the spin Hall effect in the HM. Investigations of such interfacial magnetoresistance have recently been extended to HM/antiferromagnet bilayers, such as Pt/Cr₂O₃, where the direction of the antiferromagnetic moments can be read from the resistance [17,18]. It has so far been reported that Pt/Cr₂O₃, W/Cr₂O₃, and Ta/Cr₂O₃ show a SMR-like variation in both the transverse and the longitudinal resistance [19].

*mtaka@scl.kyoto-u.ac.jp

†shiratsuchi@mat.eng.osaka-u.ac.jp

‡These authors contributed equally to this work.

However, all previous reports seem to pay less attention to the peculiar temperature dependence of the SMR-like effect in the vicinity of the Néel temperature, which cannot be accounted for if the typical temperature dependence of the magnetic susceptibility determines predominantly the behavior of the SMR. This strongly suggests that there may be an additional type of spin-dependent transport that we have been overlooking in these material systems.

In this paper, we report in-depth investigations of the spin-dependent transport in Pt/Cr₂O₃. It is found that there is a nonlinear Hall effect originating from the Pt/Cr₂O₃ interface, and its magnitude is considerably large compared with the net magnetic moments possibly residing at the interface, which are determined by use of hard and soft-X-ray magnetic circular dichroism (XMCD). Our thorough exploration reveals that the origin of the nonlinear Hall effect is due not to the SMR but to the AHE intrinsic to the Pt/Cr₂O₃ interface.

II. EXPERIMENTAL METHODS

Pt(t_{Pt})/Cr₂O₃(20 nm) bilayers ($t_{\text{Pt}} = 1, 2, 3, 5,$ and 10 nm) are fabricated on an α -Al₂O₃ (0001) substrate by dc magnetron sputtering with a base pressure below 7×10^{-7} Pa. The Cr₂O₃ is formed by sputtering of a pure Cr target in a mixture of Ar and O₂ gases with a substrate temperature of 773 K. Pt is subsequently deposited at room temperature. Epitaxial growth is confirmed by *in situ* reflection high-energy electron diffraction (RHEED). Typical RHEED images with a $[1\bar{1}\bar{2}0]_{\text{substrate}}$ azimuth obtained

for the Cr₂O₃ surface and for 1- and 2-nm-thick Pt layers are shown in Fig. 1. The RHEED pattern of the Cr₂O₃ surface is streaky, indicating a flat surface of the Cr₂O₃ layer. The diffraction pattern is explained by the corundum (0001) surface. According to the structure factor of the corundum structure, the $[1\bar{1}\bar{2}0]$ -projected reciprocal lattice of the single-crystalline corundum (0001) surface is asymmetric [20], whereas the observed RHEED pattern is symmetric with respect to the (00) streak. This symmetric RHEED pattern is a signature of a twinned Cr₂O₃(0001) film, as indicated by the key diagram in Fig. 1(d). The diffraction patterns of the Pt surface indicate epitaxial growth of Pt(111) on the Cr₂O₃(0001) surface.

For the transport measurements, the films are patterned into a Hall cross with a 5- μm -wide and 25- μm -long channel, as shown in the inset of Fig. 2(a), by conventional photolithography and Ar ion milling. The longitudinal (R_{xx}) and transverse (R_{xy}) resistances are measured as a function of the external magnetic field H , applied perpendicular to the film. The temperature is varied from 260 to 350 K, across the Néel temperature $T_N \sim 307$ K of Cr₂O₃ [21]. Hard- and soft-X-ray absorption spectroscopy (XAS) and XMCD spectroscopy are performed to determine the possible existence of a Pt-induced moment and the magnetic response of the uncompensated Cr moments at the Pt/Cr₂O₃ interface. The beamlines BL39XU (hard X-rays) and BL25SU (soft X-rays) at the SPring-8 synchrotron radiation facility are used for the XAS and XMCD measurements. The XMCD data are collected by taking the difference between the XAS spectra for left-

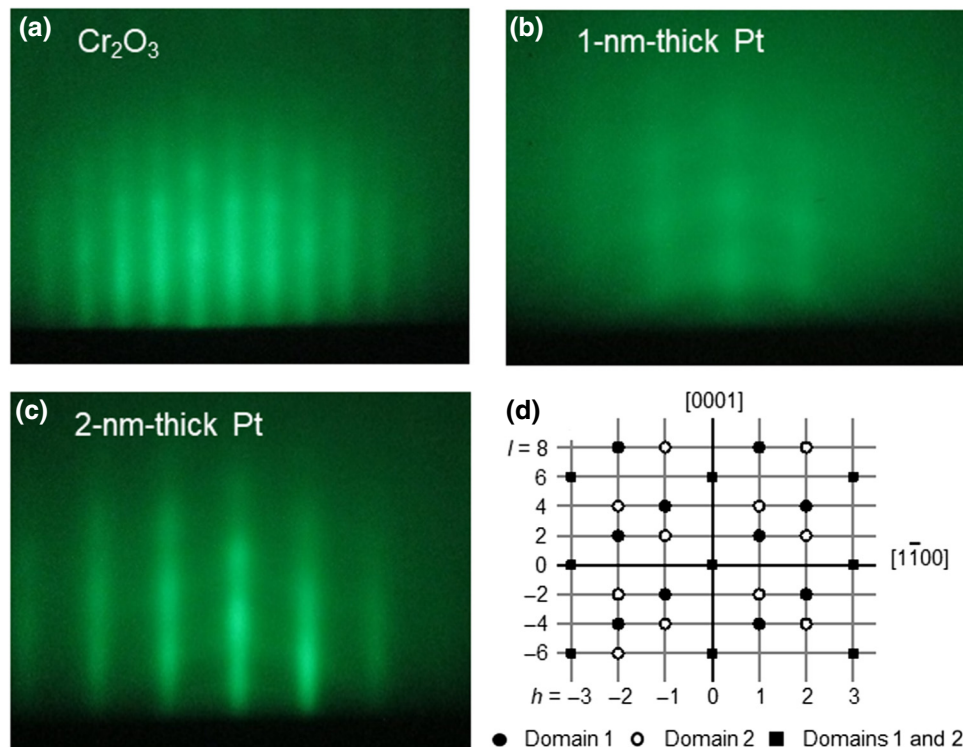


FIG. 1. RHEED patterns of (a) Cr₂O₃ surface, with a corresponding key diagram, and (b) 1-nm-thick Pt and (c) 2-nm-thick Pt layers on Cr₂O₃. The electron azimuth is $[1\bar{1}\bar{2}0]$ of the α -Al₂O₃(0001) substrate. (d) Key diagram for the Cr₂O₃ RHEED pattern.

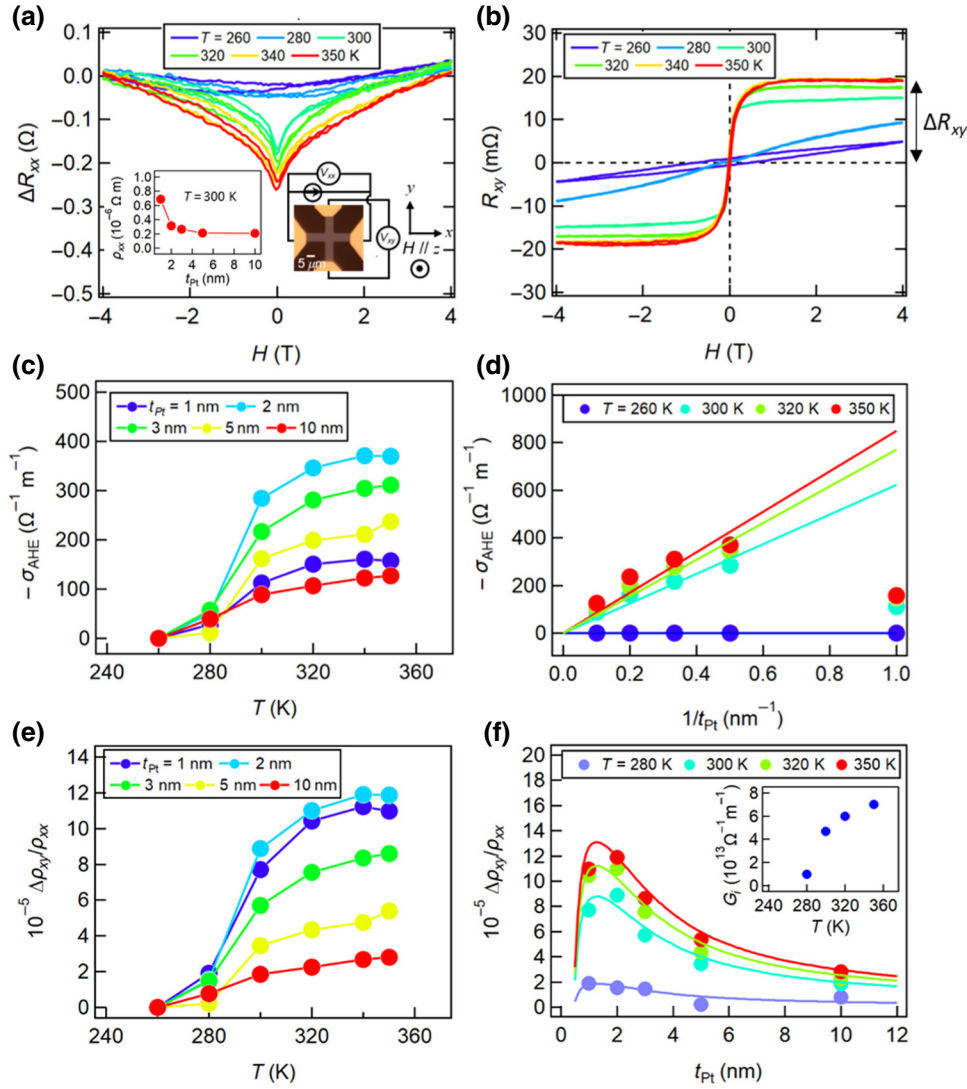


FIG. 2. (a) ΔR_{xx} and (b) R_{xy} as a function of the external field for Pt(1 nm)/Cr₂O₃(20 nm), with definition of ΔR_{xy} . The insets of (a) show an optical-microscope image of the fabricated Hall-cross pattern with a measurement diagram, and ρ_{xx} as a function of t_{Pt} . Anomalous Hall conductivity σ_{AHE} as a function of temperature (c) and as a function of $1/t_{Pt}$ (d). $\Delta\rho_{xy}/\rho_{xx}$ as a function of temperature (e) and as a function of t_{Pt} (f). The inset of (f) shows G_i , estimated from curve fitting with Eq. (1), as a function of temperature.

and right-circularly polarized X-rays, denoted by μ_+ and μ_- , respectively. Absorption signals are recorded using the fluorescence method for Pt and the total-electron-yield method at a bias voltage of -18 V for Cr. The incidence angle of the x-ray beam is 10° from the film normal. During the XMCD measurements, the magnetic field is applied out of the film plane.

III. RESULTS AND DISCUSSION

Figures 2(a) and 2(b) shows representative values of ΔR_{xx} ($=R_{xx}(H) - R_{xx}(H=4$ T)) and R_{xy} as a function of the magnetic field applied perpendicular to the sample plane for the Pt(1 nm)/Cr₂O₃(20 nm) film. At 260 K, both ΔR_{xx} and R_{xy} show a monotonic change with respect to the magnetic field. With increasing temperature, R_{xy} starts to show nonlinear behavior and saturates at about 0.5 T, resembling the AHE generally observed in a ferromagnet. ΔR_{xx} shows a rather steep increase at low fields, which seems to correlate with the behavior of R_{xy} . These

observations are in good agreement with recent reports on Pt/Cr₂O₃ systems [17,18]. We find that this saturation behavior is common to every t_{Pt} , while the value of R_{xy} at saturation, defined as ΔR_{xy} [see Fig. 2(b)], which translates to a resistivity $\Delta\rho_{xy}$, increases with decreasing t_{Pt} . We also note that the longitudinal resistivity ρ_{xx} shows a rapid increase as t_{Pt} decreases, as shown in the inset of Fig. 2(a).

Figures 2(c) and 2(d) plot the anomalous Hall conductivity σ_{AHE} ($= -\Delta\rho_{xy}/\rho_{xx}^2$) as a function of temperature and $1/t_{Pt}$. The negative Hall conductivity indicates the contribution of electron carriers to the Hall effect. We also plot the transverse magnetoresistance ratio $\Delta\rho_{xy}/\rho_{xx}$ as a function of temperature and t_{Pt} . The temperature dependence of σ_{AHE} and $\Delta\rho_{xy}/\rho_{xx}$ plotted in Figs. 2(c) and 2(e) indicates that the abrupt increase in $\Delta\rho_{xy}$, which coincides with the behavior of ρ_{xx} from which T_N can be determined [18], is related to the magnetic phase transition of Cr₂O₃ ($T_N \sim 307$ K). σ_{AHE} increases with $1/t_{Pt}$ except for the thinnest Pt layer, with $t_{Pt} = 1$ nm, for which the continuity of the Pt film is suspect, as seen from the anomalously large

ρ_{xx} seen in the inset of Fig. 2(a). This trend can be fitted with a function $1/t_{\text{Pt}}$, which indicates that the observed σ_{AHE} originates from the Pt/Cr₂O₃ interface.

We first analyze the data based on the hypothesis that the AHE is due to the SMR mechanism. According to the theory of the SMR [16], $\Delta\rho_{xy}/\rho_{xx}$ in a perpendicular field, or the spin Hall AHE, is described by

$$\frac{\Delta\rho_{xy}}{\rho_{xx}} = \frac{2\lambda^2\theta_{\text{SH}}^2}{t_{\text{Pt}}} \frac{\sigma_{xx}G_i \tanh^2(t_{\text{Pt}}/2\lambda)}{[\sigma_{xx} + 2\lambda G_r \coth(t_{\text{Pt}}/\lambda)]^2}, \quad (1)$$

where θ_{SH} , λ , and σ_{xx} ($=\rho_{xx}^{-1}$) are the spin Hall angle, the spin diffusion length, and the conductivity of Pt, respectively, and G_r and G_i are the real and imaginary parts of the mixing conductance at the Pt/Cr₂O₃ interface. Assuming that $\theta_{\text{SH}}=0.1$ [22] and $G_r=10^{14} \Omega^{-1} \text{m}^{-2}$ [23] are hypothetically independent of temperature, it is found that λ is approximately 1 nm, and a temperature-dependent $G_i=1-7 \times 10^{13} \Omega^{-1} \text{m}^{-2}$ can reproduce well

the t_{Pt} dependence of $\Delta\rho_{xy}/\rho_{xx}$, as shown by the fitting curves overlaid on Fig. 2(f) and the temperature dependence of G_i as shown in the inset of Fig. 2(f). The relatively large G_i and the strong temperature dependence cannot be reasonably explained in the framework of general interfacial spin transfer [23,24]. Even if the SMR were the origin of the observed AHE, the question would arise of what magnetic order gives rise to the SMR. Therefore, in the following, we carefully investigate possible relevant magnetic orders such as a proximity-induced Pt magnetic moment and uncompensated Cr magnetic moments.

Figure 3(a) shows the XAS and XMCD spectra at the Pt L_3 edge of the Pt(1 nm)/Cr₂O₃(20 nm) film measured at 350 K, above T_N of Cr₂O₃ (approximately 307 K). We apply a constant magnetic field of 1.3 T, which is sufficient to saturate R_{xy} [see Fig. 1(b)]. The peak position and the extended x-ray absorption fine structure are similar to those in the reported spectra for metallic Pt [25]. As seen in Fig. 3(a), the XMCD signal is virtually zero,

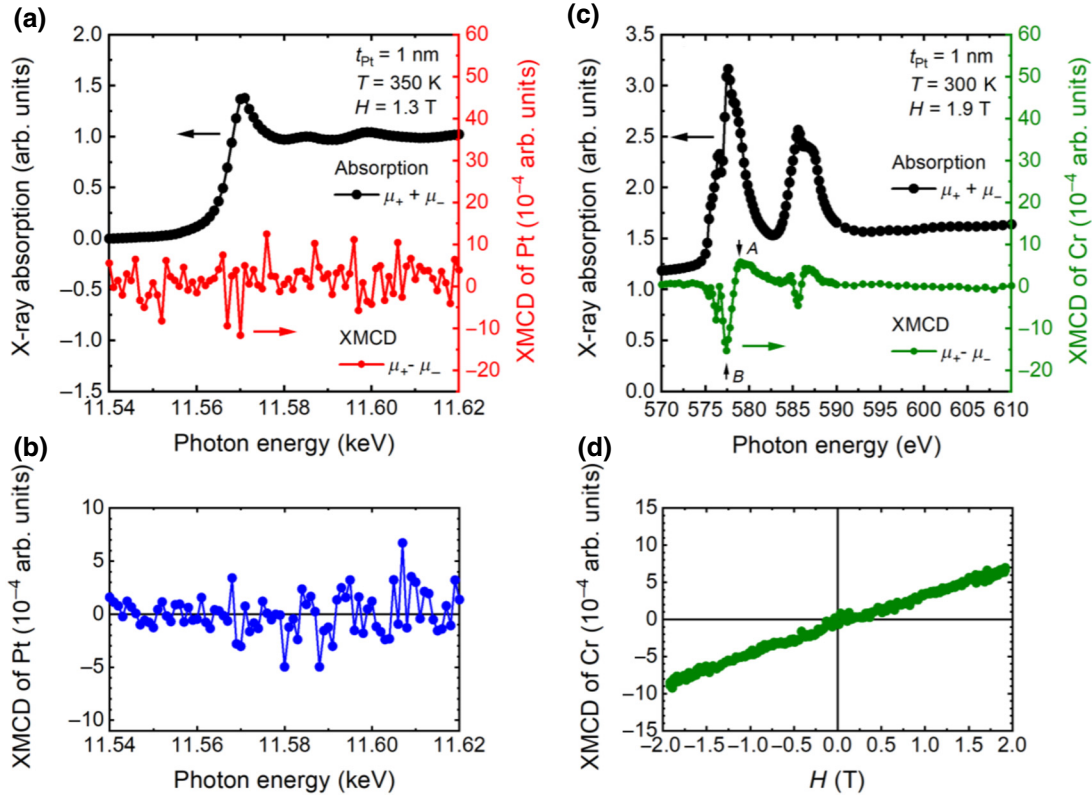


FIG. 3. (a) XAS and XMCD spectra at the Pt L_3 edge for the Pt(1 nm)/Cr₂O₃(20 nm) film. The measurement temperature is 350 K. The applied out-of-plane magnetic field during the measurements is 1.3 T. (b) XMCD spectrum at the Pt L_3 edge after MEFC, measured using Pt(1 nm)/Cr₂O₃(200 nm) prepared on a 0.5-wt % Nb-doped SrTiO₃(111) substrate. The magnetic field and voltage during the MEFC are +1.3 T and +1.2 V, respectively. The measurement temperature is 28 K. The x-ray absorption intensity and the XMCD intensity are normalized by the XAS edge jump. (c) XAS and XMCD spectra at the Cr $L_{2,3}$ edges for the Pt(1 nm)/Cr₂O₃(20 nm) film. The measurement temperature is 300 K. The applied magnetic field during the measurements is 1.9 T in the direction perpendicular to the film. (d) Magnetic field dependence of the XMCD intensity. The difference between the XMCD signals measured at the photon energies labeled A and B in (c) is taken and plotted as a function of the external field. The XMCD intensity in (d) is normalized by the total absorption intensity, $(\mu_+ - \mu_-)/(\mu_+ + \mu_-)$.

indicating that the Pt-induced moment should be below the detection limit. One may wonder whether the zero XMCD signal might be due to the multidomain state of the Cr_2O_3 , which could cause the XMCD signals to cancel out if the Pt-induced moment is associated with the Cr moments. Therefore, we take advantage of the magnetoelectric-field-cooling (MEFC) process, discussed elsewhere [26–28], to realize single-domain Cr_2O_3 and confirm the absence of a Pt-induced moment. For the experiments required for the MEFC process, we use Pt(1 nm)/ Cr_2O_3 (200 nm) films prepared on a 0.5-wt% Nb-doped SrTiO_3 (111) substrate, which are slightly different, but the film quality of the Pt/ Cr_2O_3 as checked by RHEED patterns is comparable to that of the devices that are our main interest. We find no appreciable XMCD signals of a Pt-induced moment, as shown in Fig. 3(b), even at 28 K (much less than T_N) after forming a single-domain state by MEFC with a field of +1.3 T and a voltage of +1.2 V (+6.0 MV/m). We therefore determine the upper limit of the Pt-induced moment, if exists, to be $M_{\text{Pt}} < 0.001\mu_B$ per Pt atom, considering that the maximum resolution of the XMCD intensity is approximately 0.1% of the edge jump of the XAS spectrum. Here, we assume that the induced moment is distributed throughout the whole Pt layer and that the ratio of the XMCD intensities at the L_3 and L_2 edges, namely, $m_{s, \text{eff}}/m_{\text{orb}}$ (where $m_{s, \text{eff}}$ is an effective spin moment and m_{orb} is an orbital moment), is the same as that for the Pt-induced moment at a Co/Pt interface [10]. These results suggest that the Pt-induced moment is insignificant in the Pt/ Cr_2O_3 system.

Figure 3(c) shows XAS and XMCD spectra for the Cr $L_{2,3}$ edges for the Pt(1 nm)/ Cr_2O_3 (20 nm) film measured at 300 K. The shape of the XAS spectrum indicates a single phase of Cr_2O_3 , without formation of other phases such as CrO_2 [29]. The shape of the spectrum is quite similar to that in our previous report [30,31]. In order to improve the signal-to-noise ratio, we take the difference between the values measured at the photon energies labeled A and B in Fig. 3(c) and plot it as a function of the external field in Fig. 3(d). The XMCD intensity increases linearly with increasing magnetic field in the range of ± 1.9 T. The result indicates no clear correlation between the magnetization behavior of the Cr moment and the observed Hall resistance showing nonlinear behavior [see Fig. 2(b)]. The sum-rule analysis [32,33] with a spin-correction factor [34] of the XMCD spectrum shown in Fig. 3(c) gives about $0.006\mu_B$ per Cr atom at 1.9 T. This value is well explained by the magnetic susceptibility of bulk Cr_2O_3 [21], indicating that the value of $0.006\mu_B$ is the response of the bulk antiferromagnetic moment. The data in Fig. 3(d) suggest that any possible uncompensated Cr moment, if it exists and behaves nonlinearly with respect to the field, can be estimated to be less than $0.001\mu_B$ per Cr atom.

The present results strongly indicate that there is no detectable magnetic moment induced at the interface that

could give rise to the AHE response. However, there could be a possible mechanism that does not involve the net magnetic moment, similarly to the case for the AHE in the noncollinear antiferromagnet Mn_3Sn [5–7]. The AHE that we observe may be associated with the field response of a nontrivial magnetic texture with a negligible net magnetic moment. It should be noted that, considering the maximum size of the net magnetic moment possibly residing at the interface, the Hall conductivity found in this study is considerable. The Hall conductivity per unit net magnetic moment is calculated to be $-\sigma_{\text{AHE}}/M = 350$ ($\Omega^{-1} \text{m}^{-1}$)/ $0.001\mu_B$ (J T^{-1} per magnetic atom) = 0.57 V^{-1} , which is quite large compared with the values for general magnetic materials [5].

In order to identify the origin of our observed AHE, we carry out first-principles calculations [35–37] together with use of the Kubo formula based on linear response theory [38] to derive the intrinsic anomalous Hall conductivity σ'_{AHE} . The Pt/ Cr_2O_3 bilayer is modeled by a two-atomic-layer film of Pt(111) on a 12-atomic-layer film of Cr_2O_3 (0001) as depicted in Figs. 4(a) and 4(b). The in-plane lattice constant is assumed to be that of bulk Cr_2O_3 , and the Cr-terminated surface structure is determined by an analysis of the surface formation energy [39]. The lattices of the Pt and the Cr_2O_3 (0001) in the first five atomic layers from the interface are fully relaxed by atomic-force calculations.

To explore the effect of the Pt/ Cr_2O_3 interface, we calculate σ'_{AHE} by varying the interlayer distance between the Pt and Cr_2O_3 layers. When the interlayer distance is virtually set to infinity, i.e., we assume a freestanding Pt film with the lattice constant of bulk Pt, we obtain a positive correlation between the calculated anomalous Hall conductivity and the spin magnetic moments in the Pt induced by a given applied field, as shown in Fig. 4(c). It is also found that σ'_{AHE} is much enhanced when the Pt/ Cr_2O_3 interface is properly taken into account [see Fig. 4(c)]. We also find that σ'_{AHE} decreases drastically when the interlayer distance is increased by just 1 Å from the relaxed value [see also Fig. 4(c)]. Although the calculation tends to overestimate the spin magnetic moment of the Pt compared with the experimentally estimated value (less than $0.001\mu_B$), it clearly reveals that σ'_{AHE} can vary drastically with subtle details of the condition of the Pt/ Cr_2O_3 interface.

By exploring the band structure, σ'_{AHE} is found to arise from the bands around E_F at the K -point, as shown in Figs. 4(d) and 4(e). The spin-orbit coupling opens up a small energy gap, at the K -point at E_F , in the bands consisting mainly of Pt d orbitals, which leads to a large Berry curvature. Figure 4(e) plots σ_{AHE} along some k -directions by integrating the Berry curvature up to E_F . This clearly shows a large peak in the AHE contribution around the K -point. It is also found that the magnetic moment coupled to these bands at around the K -point is slightly canted

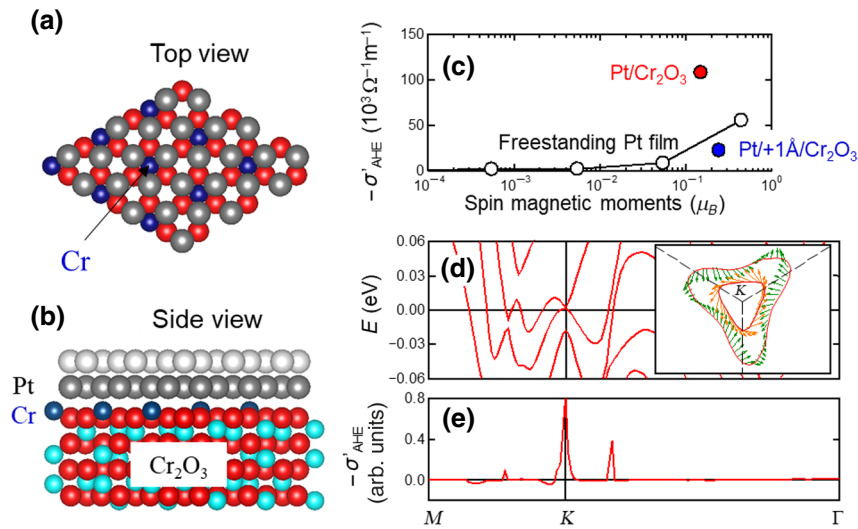


FIG. 4 (a),(b) Top and side views of calculated interface structure of Pt/Cr₂O₃. (c) Relation between σ'_{AHE} and the spin magnetic moments of Pt at the interface in Pt/Cr₂O₃, where the red and blue solid circles represent results for the fully optimized interface structure and when the interlayer distance between the Pt and Cr₂O₃ films is changed by 1 Å [Pt/(+1 Å)/Cr₂O₃]. The open circles show the AHE as a function of the spin magnetic moment in a freestanding Pt film consisting of two atomic (111) layers. (d) Band structure and (e) variation of σ'_{AHE} along the high-symmetry k directions. The inset of (d) shows two constant-energy contours around the K -point in the two-dimensional Brillouin zone, at 7 meV above (yellow) and 3 meV below (green) E_F , where arrows indicate the in-plane components of the spin magnetic moments.

toward the in-plane direction, while the net spin magnetic moment is oriented along the out-of-plane direction. The in-plane components of the spin magnetic moments, as shown by the arrows in the inset of Fig. 4(d), lie on the two constant-energy contours around the K -point at 7 meV above (yellow) and 3 meV below (green) E_F . The results thus illustrate two spin-chiral textures with opposite chirality in the bands across E_F , which are likely responsible for an intrinsic AHE [40] that does not rely on the net magnetic moment. We note that the skew-scattering mechanism in spin-chiral textures under thermal fluctuations, recently proposed by Kato *et al.* using a Monte Carlo simulation [41], should also contribute to the observed large σ_{AHE} , which may indeed explain the enhancement of σ_{AHE} above T_N [e.g., Fig. 2(c)]. Further clarification of the temperature dependence and field dependence of the spin-chiral texture and therefore of the σ_{AHE} observed in our experiments, although it is beyond our present first-principles calculations, is a theoretical challenge to be addressed.

IV. CONCLUSIONS

In summary, we investigate the spin-dependent transport in Pt/Cr₂O₃, focusing especially on the Hall resistance as a function of the external magnetic field. It is found that there is a nonlinear AHE originating from the Pt/Cr₂O₃ interface and that its magnitude is considerable compared with the interfacial magnetic moments determined by XMCD measurements. The upper limit on the

possible net magnetic moment M of $0.001\mu_B$ yields a Hall conductivity per unit net magnetic moment $-\sigma_{\text{AHE}}/M$ of 0.57 V^{-1} , which is extraordinary large compared with the values for general magnetic materials. First-principles calculations reveal that there are spin-chiral textures in the energy bands associated with the Pt/Cr₂O₃ interface. This suggests the existence of an intrinsic AHE at the Pt/Cr₂O₃ interface due to a nontrivial magnetic texture. While the SMR mechanism limits the maximum Hall conductivity because of the magnitude of the spin Hall angle, the mechanism of the AHE due to interfacial chiral magnetism could be used to further enhance the anomalous Hall conductivity by interfacial engineering, which may be found useful in spintronic applications such as magnetic sensing and storage.

ACKNOWLEDGMENTS

The XMCD measurements are performed at BL39XU and BL25SU at the SPring-8 synchrotron radiation facility with the approval of the Japan Synchrotron Radiation Research Institute (JASRI) (Proposals No. 2013A1751, No. 2015A1215, No. 2017A1212, and No. 2017B0079). This work is partly supported by JSPS KAKENHI (Grants No. 17K18991, No. 17H05181, and No. 17H04924).

[1] C. L. Chien and C. R. Westgate, *The Hall Effect and Its Applications* (Plenum, New York, 1980).

- [2] N. Nagaosa, J. Sinova, S. Onoda, A. H. MacDonald, and N. P. Ong, Anomalous Hall effect, *Rev. Mod. Phys.* **82**, 1539 (2010).
- [3] Z. Fang, et al., The anomalous Hall effect and magnetic monopoles in momentum space, *Science* **302**, 92 (2003).
- [4] G. Koster, L. Klein, W. Siemons, G. Rijnders, J. S. Dodge, C.-B. Eom, D. H. A. Blank, and M. R. Beasley, Structure, physical properties, and applications of SrRuO₃ thin films, *Rev. Mod. Phys.* **84**, 253 (2012).
- [5] S. Nakatsuji, N. Kiyohara, and T. Higo, Large anomalous Hall effect in a non-collinear antiferromagnet at room temperature, *Nature* **527**, 212 (2015).
- [6] H. Chen, Q. Niu, and A. H. MacDonald, Anomalous Hall Effect Arising From Noncollinear Antiferromagnetism, *Phys. Rev. Lett.* **112**, 017205 (2014).
- [7] N. Kiyohara, T. Tomita, and S. Nakatsuji, Giant Anomalous Hall Effect in the Chiral Antiferromagnet Mn₃Ge, *Phys. Rev. Appl.* **5**, 064009 (2016).
- [8] S. Rüegg, G. Schütz, P. Fischer, R. Wienke, W. B. Zeper, and H. Ebert, Spin-dependent x-ray absorption in Co/Pt multilayers, *J. Appl. Phys.* **69**, 5655 (1991).
- [9] G. Schütz, S. Stähler, M. Knülle, P. Fischer, S. Parkin, and H. Ebert, Distribution of magnetic moments in Co/Pt and Co/Pt/Ir/Pt multilayers detected by magnetic x-ray absorption, *J. Appl. Phys.* **73**, 6430 (1993).
- [10] M. Suzuki, H. Muraoka, Y. Inaba, H. Miyagawa, N. Kawamura, T. Shimatsu, H. Maruyama, N. Ishimatsu, Y. Isohara, and Y. Sonobe, Depth profile of spin and orbital magnetic moments in a subnanometer Pt film on Co, *Phys. Rev. B* **72**, 054430 (2005).
- [11] A. Fert, V. Cros, and J. Sampaio, Skyrmions on the track, *Nat. Nanotechnol.* **8**, 152 (2013).
- [12] I. M. Miron, G. Gaudin, S. Auffret, B. Rodmacq, A. Schuhl, S. Pizzini, J. Vogel, and P. Gambardella, Current-driven spin torque induced by the Rashba effect in a ferromagnetic metal layer, *Nat. Mater.* **9**, 230 (2010).
- [13] M. I. D'yakonov and V. I. Perel, Possibility of orienting electron spins with current, *JETP Lett.* **13**, 467 (1971).
- [14] L. Liu, C.-F. Pai, Y. Li, H. W. Tseng, D. C. Ralph, and R. A. Buhrman, Spin-torque switching with the giant spin Hall effect of tantalum, *Science* **336**, 555 (2012).
- [15] H. Nakayama, M. Althammer, Y.-T. Chen, K. Uchida, Y. Kajiwara, D. Kikuchi, T. Ohtani, S. Geprägs, M. Opel, S. Takahashi, P. Gross, G. E. W. Bauer, S. T. B. Goennenwein, and E. Saitoh, Spin Hall Magnetoresistance Induced by a Nonequilibrium Proximity Effect, *Phys. Rev. Lett.* **110**, 206601 (2013).
- [16] Y.-T. Chen, S. Takahashi, H. Nakayama, M. Althammer, S. T. B. Goennenwein, E. Saitoh, and G. E. W. Bauer, Theory of spin Hall magnetoresistance, *Phys. Rev. B* **87**, 144411 (2013).
- [17] Y. Ji, J. Miao, Z. Y. Ren, B. W. Dong, X. G. Xu, Y. Wu, and Y. Jiang, Spin Hall magnetoresistance in an antiferromagnetic magnetoelectric Cr₂O₃/heavy-metal W heterostructure, *Appl. Phys. Lett.* **110**, 262401 (2017).
- [18] T. Iino, T. Moriyama, H. Iwaki, H. Aono, Y. Shiratsuchi, and T. Ono, Resistive detection of the Néel temperature of Cr₂O₃ thin films, *Appl. Phys. Lett.* **114**, 022402 (2019).
- [19] Y. Ji, J. Miao, Y. M. Zhu, K. K. Meng, X. G. Xu, J. K. Chen, and Y. Jiang, Negative spin Hall magnetoresistance in antiferromagnetic Cr₂O₃/Ta bilayer at low temperature region, *Appl. Phys. Lett.* **112**, 232404 (2018).
- [20] A. Stierle, Th. Koll, and H. Zabel, Structure and defects of epitaxial overlayers on Cr(110), *Phys. Rev. B* **58**, 5062 (1998).
- [21] S. Foner, High-field antiferromagnetic resonance in Cr₂O₃, *Phys. Rev.* **130**, 183 (1963).
- [22] H. L. Wang, C. H. Du, Y. Pu, R. Adur, P. C. Hammel, and F. Y. Yang, Scaling of Spin Hall Angle in 3d, 4d, and 5d Metals From Y₃Fe₅O₁₂/Metal Spin Pumping, *Phys. Rev. Lett.* **112**, 197201 (2014).
- [23] X. Jia, K. Liu, K. Xia, and G. E. W. Bauer, Spin transfer torque on magnetic insulators, *Europhys. Lett.* **96**, 17005 (2011).
- [24] L. Ma, L. Lang, J. Kim, Z. Yuan, R. Wu, S. Zhou, and X. Qiu, Spin diffusion length and spin Hall angle in Pd1-xPt_x/YIG heterostructures: Examination of spin relaxation mechanism, *Phys. Rev. B* **98**, 224424 (2018).
- [25] A. V. Kolobov, F. Wilhelm, A. Rogalev, T. Shima, and J. Tominaga, Thermal decomposition of sputtered thin PtO_x layers used in super-resolution optical disks, *Appl. Phys. Lett.* **86**, 121909 (2005).
- [26] P. Borisov, A. Hochstrat, X. Chen, W. Kleemann, and C. Binck, Magnetoelectric Switching of Exchange Bias, *Phys. Rev. Lett.* **94**, 117203 (2005).
- [27] T. Ashida, M. Oida, N. Shimomura, T. Nozaki, T. Shibata, and M. Sahashi, Observation of magnetoelectric effect in Cr₂O₃/Pt/Co thin film system, *Appl. Phys. Lett.* **104**, 152409 (2014).
- [28] K. Toyoki, Y. Shiratsuchi, T. Nakamura, C. Mitsumata, S. Harimoto, Y. Takechi, T. Nishimura, H. Nomura, and R. Nakatani, Equilibrium surface magnetization of α -Cr₂O₃ studied through interfacial chromium magnetization in Co/ α -Cr₂O₃ layered structures, *Appl. Phys. Express* **7**, 114201 (2014).
- [29] Y. Yamazaki, T. Kataoka, V. R. Singh, A. Fujimori, F.-H. Chang, D.-J. Huang, H.-J. Lin, C. T. Chen, K. Ishikawa, K. Zhang, and S. Kuroda, Observation of magnetoelectric effect in Cr₂O₃/Pt/Co thin film system, *J. Phys.: Condens. Matter* **23**, 176002 (2011).
- [30] Y. Shiratsuchi, W. Kuroda, T. V. A. Nguyen, Y. Kotani, K. Toyoki, T. Nakamura, M. Suzuki, K. Nakamura, and R. Nakatani, Simultaneous achievement of high perpendicular exchange bias and low coercivity by controlling ferromagnetic/antiferromagnetic interfacial magnetic anisotropy, *J. Appl. Phys.* **121**, 073902 (2017).
- [31] Y. Shiratsuchi, H. Noutomi, H. Oikawa, T. Nakamura, M. Suzuki, T. Fujita, K. Arakawa, Y. Takechi, H. Mori, T. Kinoshita, M. Yamamoto, and R. Nakatani, Detection and in Situ Switching of Unreversed Interfacial Antiferromagnetic Spins in a Perpendicular-Exchange-Biased System, *Phys. Rev. Lett.* **109**, 077202 (2012).
- [32] B. T. Thole, P. Carra, F. Sette, and G. van der Laan, X-ray Circular Dichroism as a Probe of Orbital Magnetization, *Phys. Rev. Lett.* **68**, 1943 (1992).
- [33] P. Carra, B. T. Thole, M. Altarelli, and X. Wang, X-ray Circular Dichroism and Local Magnetic Fields, *Phys. Rev. Lett.* **70**, 694 (1993).
- [34] E. Goering, X-ray magnetic circular dichroism sum rule correction for the light transition metals, *Phil. Mag.* **85**, 2895 (2005).

- [35] The full-potential linearized augmented plane wave method is adopted for the first-principles calculations [36]. The calculations are done with a local-density approximation using the correlation correction $+U$ for the Cr atoms ($U = 4.0$ eV and $J = 0.58$ eV [37]). The spin-orbit coupling is treated by the second variational method. For the generation of the magnetic moment in the Pt layer, a magnetic Zeeman field H_{SZ} is implemented in the Kohn-Sham Hamiltonian. See Ref. [36] for more details of the methodology.
- [36] K. Nakamura, T. Ito, A. J. Freeman, L. Zhong, and J. Fernandez-de-Castro, Intra-atomic noncollinear magnetism and the magnetic structures of antiferromagnetic FeMn, *Phys. Rev. B* **67**, 014405 (2003); K. Nakamura, K. Hatano, T. Akiyama, T. Ito, and A. J. Freeman, Lattice expansion, stability, and Mn solubility in substitutionally Mn-doped GaAs, *Phys. Rev. B* **75**, 205205 (2007).
- [37] S. Shi, A. L. Wysocki, and K. D. Belashchenko, Magnetism of chromia from first-principles calculations, *Phys. Rev. B* **79**, 104404 (2009).
- [38] G. Y. Guo, S. Murakami, T.-W. Chen, and N. Nagaosa, Intrinsic Spin Hall Effect in Platinum: First-Principles Calculations, *Phys. Rev. Lett.* **100**, 096401 (2008).
- [39] A. Rohrbach, J. Hafner, and G. Kresse, Ab initio study of the (0001) surfaces of hematite and chromia: Influence of strong electronic correlations, *Phys. Rev. B* **70**, 125426 (2004).
- [40] L. Fu, Hexagonal Warping Effects in the Surface States of the Topological Insulator Bi_2Te_3 , *Phys. Rev. Lett.* **103**, 266801 (2009).
- [41] Y. Kato and H. Ishizuka, Colossal Enhancement of Spin-Chirality-Related Hall Effect by Thermal Fluctuation, *Phys. Rev. Appl.* **12**, 021001 (2019).